3-D Coastal Bathymetry Simulation from Airborne TOPSAR Polarized Data

Maged Marghany
Institute for Science and Technology Geospatial (INSTEG),
Universiti Teknologi Malaysia, Skudai, Johore Bahru
Malaysia

1. Introduction

Remote sensing techniques in real time could be a major tool for bathymetry mapping which could produce synoptic data overlarge areas at extremely low cost. In contrast, conventional techniques such as single- or multi-beam ship-borne echoes are costly and time-consuming, especially when large areas are being surveyed (Marghany et al., 2009b). The ocean bathymetry features can image by radar in coastal waters with strong tidal currents (Vogelzang et al., 1992; Vogelzang et al., 1997; Hesselmans et al., 2000, Marghany et al., 2010). Under practical circumstances, synthetic aperture radar (SAR) is able to detect shallow ocean bathymetry features (Alpers and Hennings 1984; Shuchman et al. 1985; and Vogelzang 1997). According to Alpers and Henning (1984) ocean bathymetry can determine indirectly based on means of sea surface variations that caused by the gradient current overflowing the submarine features. Therefore, this concept is valid with the presence of strong current associates with capillary waves. Under this circumstance, SAR antenna receives a strong backscatter from ocean surface. Nevertheless, multi-beam ship-borne echoes provide bathymetry to water depths above 100 m whereas SAR data are limited to less than 25 m. Under local circumstances such as strong tidal gradient and wind speed higher than 3 m/s, SAR data can detect shallow ocean bathymetry features down to 20 m (Marghany et al., 2009b).

1.1 Principle of SAR ocean bathymetry imaging

Several theories concerning the radar imaging mechanism of underwater bathymetry have been established, such as by Alpers and Hennings (1984); Shuchman et al. (1985); and Vogelzang (1997). The physical theories describing the radar imaging mechanisms for ocean bathymetry are well understood as three stages: (i) the modulation of the current by the underwater features, (ii) the modulation of the sea surface waves by the variable surface current, and (iii) the interaction of the microwaves with the surface waves (Alpers and Hennings, 1984) (Fig. 1). The imaging mechanism which reflects sea bottom topography in a given SAR image consists of three models. These models are a flow model, a wave model and the SAR backscatter model. These theories are the basis of commercial services which generate bathymetric charts by inverting SAR images at a significantly lower cost than conventional survey techniques (Wensink and Campbell, 1997). In this context, Hesselmans

et al. (2000) developed the Bathymetry Assessment System, a computer program which can be used to calculate the depth from any SAR image and a limited number of sounding data points. They found that the imaging model was suitable for simulating a SAR image from the depth map.

It showed good agreement between the backscatter in both the simulated and airborne-acquired images, when compared, with accuracy (root mean square) error of $\pm$ 0.23 m of order of 10 m within a coastal bathymetry range of 25-30 m. Recently, Li et al., (2009) are utilized RADARSAT-1 and ENVISAT synthetic aperture radar (SAR) images for mapping sand ridges with 30 m water depth. In doing so, they used modelled tidal current as to an advanced radar-imaging model to simulate the SAR image at a given satellite look angle and for various types of bathymetry. In this regard, the shallow-water bathymetry is acquired in a 2-D space. Finally, they reported that the sand ridge can be imaged when strong ocean currents exist. On the contrary, Lyzenga et al., (2006) used a simple method of estimating water depths from multispectral imagery, based on an approximate shallow-water reflectance model. They found that a single set of coefficients derived from a set of IKONOS images produces the good performance with an aggregate RMS error of $\pm$ 2.3 m which is higher than bathymetry retrieved from SAR (Hesselmans et al. 2000). Coastal bathymetry mapping by using optical remote sensing data, however, can be only fully utilized in the clearest water, and considerably less in turbid water (Vogelzang et al., 1992). Indeed, as the different wavelengths pass through the water column they become attenuated by the interaction with suspended particles in water (Mills, 2008).
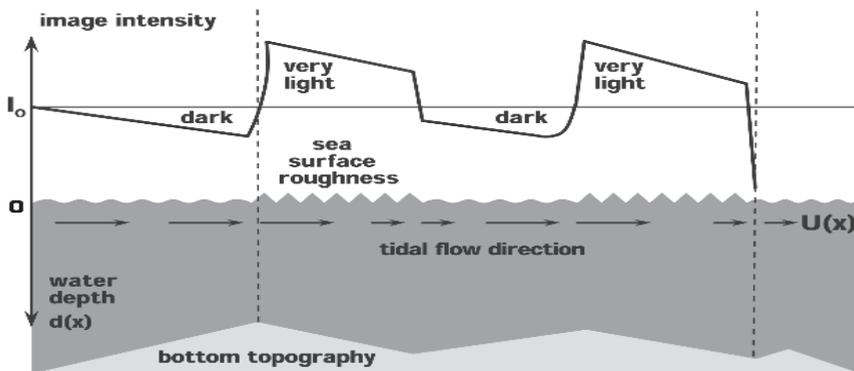

Fig. 1. SAR 's concept for imaging ocean bathymetry ((Alpers and Hennings, 1984).

1.2 Speckle impact on SAR ocean bathymetry imaging

The high speckle noise in SAR images has posed great difficulties in inverting SAR images for simulating coastal bathymetry. Speckle is a result of coherent interference effects among scatterers which are randomly scattered within each resolution cell. The speckle size, which is a function of the spatial resolution, induces errors in bathymetry signature detection. Reducing the speckle effects, require appropriate filters, i.e. Lee, Gaussian, etc. (Lee et al 2002, Marghany and Mazlan 2010), could be used in the pre-processing stage. The effectiveness of these speckle-reducing filters is however much influenced by cause's factors and application. Since the SAR images the sea surface, all speckles in SAR images are to

function of local changes in the surface roughness because, direct reduction of the wave height (because of slicks), wind impelled roughness changes (atmospheric effects) or wave-current interactions (fronts and bathymetry).

In contrast, Yu and Scott (2002) stated several restrictions of the speckle filtering approach. They reported size and shape of the filter window can affect the accuracy of despeckle filters. For instance, extremely large window size will form a blurred image, while a small window will decrease the smoothing competence of the filter and will leave speckle. They also found that window size can change the physical characteristics of targets in SAR image. For instance a square window (as is typically applied) will lead to corner rounding of rectangular features. Despite using despeckle filters to perform edge enhancement, speckle in the neighborhood of an edge (or in the neighborhood of a point feature with high contrast) will remain after filtering. Additionally, the thresholds used in the enhanced filters, although motivated by statistical arguments, are *ad hoc* improvements that only demonstrate the insufficiency of the window-based approaches. The hard thresholds that enact neighborhood averaging and identity filtering in the extreme cases lead to blotching artifacts from averaging filtering and noisy boundaries from leaving the sharp features unfiltered (Yu and Scott 2002).

In the case of bathymetry mapping not all the filters stated in the literature are suitable for bathymetry application. In fact, SAR data have discontinuities and lower grey levels gradient (Marghany et al., 2009a). Besides, by applying some kinds of filter such as Lee, most of bathymetry signature information will be lost. In this perspective, Inglada and Garello, (1999) and Marghany et al., (2009b) stated that an anisotropic diffusion filter is more appropriate for speckle reduction in the case of bathymetry signature detection in a SAR image. They concluded that it produced the highest smoothed image as the anisotropic diffusion filter preserves the mean grey-level and maintains the bathymetry signature compared to Lee filter. Nevertheless, Inglada and Garello, (1999 and 2002) were not able to state the accuracy rate of utilizing the Volterra model (Section 4.2) and anisotropic diffusion filter for SAR.

1.3 Hypothesis of study

Concerning with above prospective, we address the question of despeckles' impact on the accuracy of retrieving ocean bathymetry without needing to include any sounding data values. This was demonstrated with airborne SAR data (namely the TOPSAR) using integration of the Volterra kernel (Inglada and Garello, 1999) and fuzzy B-spline algorithm (Marghany and Mazlan 2005 and Marghany et al., 2007). Nonetheless, the studies of Marghany and Mazlan (2006) and Marghany et al., (2007) have failed to derive accurate bathymetry depth with single Cvv band although the root mean square error is ± 9 m. Five hypotheses are examined:

- the Volterra model can use to detect tidal current pattern from TOPSAR polarised data,
- anisotropic diffusion algorithm can reduce the speckle in SAR data and determine sharp bathymetry feature;
- there are significant differences between the different bands in detecting ocean currents,
- the continuity equation can be used to obtain the water depth, and
- fuzzy B-splines can be implemented to invert the water depth values determined by the continuity equation into 3-D bathymetry.

2. Study area

The study area is located in the coast of Kuala Terengganu, on eastern part of Malaysia Peninsula. This area is approximately 20 km along the north of Kuala Terengganu coastline, located between 5^0 21' N , 103^0 10' E and 5^0 30' N, 103^0 20' E). Sand materials make up the entire of this beach (Marghany 1994). The east coast of Peninsular Malaysia is annually subjected to the northeast monsoon wind (November to January) (Marghany et al., 2010) showed that the mean, and longer significant wave periods were 8 to 10 seconds.

Significant wave height maximum were reported as 4 m and 2.4 m, respectively in February and March. However, during the south-west monsoon wave height was ranged between 0.4m -0.7m (Marghany et al., 2010). During the inter- monsoon period (September to mid of November), the wave height was ranged between 0.37 m to 1.6 m (Marghany et al., 2010). According to Marghany et al., (2010) the coastal water less than 50 nautical miles from shore is quite shallow with the deepest area being approximately 50 m (Fig. 2). The bottom has gentle slopes, gradually deepening towards the open sea. A clear feature of this area is the primary hydrologic communications between the estuary and the South China Sea which is the largest estuary along the Kuala Terengganu (Marghany et al., 2009b).
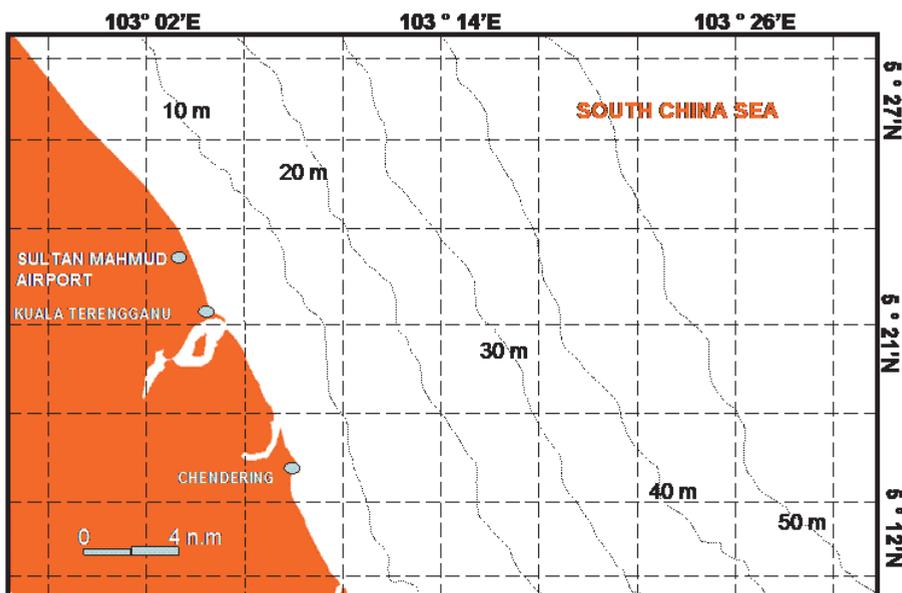

Fig. 2. Bathymetry along the coastal waters of Kuala Terengganu.

3. Data sets

Airborne data acquired in this study were derived from the Jet Propulsion Laboratory (JPL) airborne Topographic Synthetic Aperture Radar (TOPSAR) data on December 6 ,1996. TOPSAR is a NASA/JPL multi-frequency radar imaging system aboard a DC-8 aircraft and operated by NASA's Ames Research Center at Moffett Field, USA. TOPSAR data are fully

polarimetric SAR data acquired with HH-,VV-, HV- and VH-polarized signals from 5 m x 5 m pixels, recorded for three wavelengths: C band (5 cm), L band (24 cm) and P band (68 cm). The full set of C-band and L-band have linear polarizations (HH, VV, HV), phase differences (HHVV), and circular polarizations (RR, RL).

In addition, the TOPSAR sensor uses two antennas to receive the radar backscatter from the surface. The difference in arrival times of the return signals at the two antennas is converted into a modulo -2π phase difference. Further, TOPSAR data with C-band provides digital elevation model with rms error in elevation ranging from about 1 m in the near range to greater than 3 m in the far range. A further explanation of TOPSAR data acquisition is given by Melba et al. (1999). This study utilizes both Cvv and L_{HH} bands for 3-D bathymetry reconstruction because of the widely known facts of the good interaction of VV and HH polarization to oceanographic physical elements such as ocean wave, surface current features, etc. Elaboration of such further explanation can be found in (Alpers and Hennings 1984; and Inglada and Garello 2002; Marghany et al., 2010).

4. Model for 3-D bathymetry retrieving

Three models involved for 3-D bathymetry retrieving from TOPSAR polarized data: anisotropic diffusion, algorithm the Volterra model and the fuzzy B-spline model. The Volterra model is used to assimilate the tidal current flow from TOPSAR data. The simulation current velocity aims to retrieve water depth gradients under tidal current flow spatial variations. The fuzzy B-spline used to remodel the three-dimensional (3-D) water depth from a 2-D continuity equation.

4.1 Anisotropic diffusion algorithm

Anisotropic diffusion is technique that aims at reducing image noise while preserving edges, lines and other details that are important for the image interpretation (Perona and Malik 1990). Formally, let $\Omega \subset \mathbb{R}^2$ denote a subset of the TOPSAR image plane $I_{TOPSAR}(.,t) : \Omega \rightarrow \mathbb{R}$ which is part of TOPSAR intensity. Therefore, anisotropic diffusion is given by

$$\frac{\partial I_{TOPSAR}}{\partial t} = div(c(i,j,t)\Delta I_{TOPSAR})$$
$$= \nabla c . \nabla I_{TOPSAR} + c(i,j,t)\Delta I_{TOPSAR} \tag{1}$$

where, $c(i,j,t)$ is the diffusion coefficient and $c(i,j,t)$ controls the rate of diffusion that is usually chosen as a function of the TOPSAR image intensity gradient ΔI_{TOPSAR} to preserve bathymetry edge in TOPSAR data. Besides, Δ denotes the Laplacian, ∇ denotes the gradient, and $div (.......)$is the divergence operator. Following Perona and Malik (1987), two functions for the diffusion coefficient are considered:

$$c(\|\nabla I_{TOPSAR}\|) = e^{-(\|\nabla I_{TOPSAR}\|/K)^2} \tag{2}$$

and

$$c(\|\nabla I_{TOPSAR}\|) = (1 + \|\nabla I_{TOPSAR}\|)^{-1} \tag{3}$$

the constant K controls the sensitivity to edges and is usually chosen as a function of the speckle variations in TOPSAR data. In this regard, $c(\|\nabla I_{TOPSAR}\| \to 0$ if $\|\nabla I_{TOPSAR}\| \gg K$ that leads to all-pass filter. Besides isotropic diffusion (Gaussian filtering achieves under boundary condition of $c(\|\nabla I_{TOPSAR}\| \to 1$ when $\|\nabla I_{TOPSAR}\| \ll K$. Anisotropic diffusion resembles the process that creates a scale-space, where an image generates a parameterized family of successively more and more blurred images based on a diffusion process (Sapiro 2001).

4.2 Volterra algorithm

According to Marghany et al., (2010), the Volterra algorithm can use to express the SAR image intensity as a series of nonlinear filters on the ocean surface current. This means the Volterra algorithm can use to study the image energy variation as a function of parameters such as the current direction, or the current magnitude. A generalized, nonparametric framework to describe the input–output x and y signals relation of a time-invariant nonlinear system is provided by Inglada and Garello (1999). Additional, the input x corresponds to the different TOPSAR band intensities i.e., (C and L bands) whereas y corresponds to Volterra series of the different bands. In discrete form, the Volterra series for input, TOPSAR data intensities $X(n)$, and output of TOPSAR signals in form of Volterra series, $Y(n)$ as given by Inglada and Garello (2002) can be expressed as:

$$
\begin{aligned}
Y(n) = h_0 &+ \sum_{i_1=1}^{\infty} h_1(i_1)X(n-i_1) + \sum_{i_1=1}^{\infty}\sum_{i_2=1}^{\infty} h_2(i_1,i_2)X(n-i_1)X(n-i_2) + \\
&\sum_{i_1=1}^{\infty}\sum_{i_2=1}^{\infty}\sum_{i_3=1}^{\infty} h_3(i_1,i_2,i_3)X(n-i_1)X(n-i_2)X(n-i_3) + \ldots\ldots + \\
&\sum_{i_1=1}^{\infty}\sum_{i_2=1}^{\infty}\ldots\ldots\ldots\ldots\sum_{i_k=1}^{\infty} h_k(i_1,i_2,\ldots\ldots,i_k)X(n-i_1)X(n-i_2)\ldots\ldots\ldots X(n-i_k)
\end{aligned}
\tag{4}
$$

where, n, i_1, $i_2,\ldots,i_k$ are discrete time lags. The function h_k $(i_1, i_2, \ldots, i_k)$ is the kth-order Volterra kernel characterizing the system. h_1 is the kernel of the first order Volterra functional, which performs a linear operation on the input and h_2, $h_3,\ldots,h_k$ capture the nonlinear interactions between input and output TOPSAR signals. In this context, the nonlinearity is expressed as the relationship between different TOPSAR band intensities and ocean surface roughness. Consequently, surface current gradients in shallow waters can be imaged by TOPSAR different bands through energy transfer towards the waves. Indeed, the radar system is restricted to measure surface roughness. The order of the non-linearity is the highest effective order of the multiple summations in the functional series (Marghany et al., 2009b).

Following Marghany and Mazlan (2006); Marghany et al., (2009b) and Marghany et al., (2010) Fourier transform is used to acquire nonlinearity function from equation 4 as given by

$$
Y(v) = FT[Y(n)] = \int Y(n)e^{-j2\pi vn}dn
\tag{5}
$$

where, v is frequency and $j = \sqrt{-1}$ (Marghany et al., 2010). Domain frequency of TOPSAR image $I_{TOPSAR}(v,\Psi)$ can be described by using equation 5 with following expression

$$I_{TOPSAR}(v, \Psi_0) = FT[I(r,a)e^{j(R/V)u_d(r,a)}] \tag{6}$$

where $I(r,a)$ is the intensity TOPSAR image pixel of azimuth *(a)* and range *(r)*, respectively, ψ_0 is the wave spectra energy and *R/V* is the range to platform velocity ratio, in case of TOPSAR equals 32 s and $U_d(r,a)$ is the radial component of surface velocities (Inglada and Garello 2002). Marghany et al., (2010) stated that equation 6 does not satisfy the relationship between TOPSAR data and ocean surface roughness. More precisely, the action balance equation (ABE) describes the relationship between surface velocity $\bar{u}$, and its gradient and the action spectral density ψ of the short surface wave i.e. Bragg wave (Alpers and Hennings 1984). In reference to Inglada and Garello (1999), the expression of ABE into first-order Volterra kernel $H_1(v_a, v_r)$ of frequency domain for the current flow in the range direction can be described as:

$$H_1(v_a, v_r) = k_r \langle \vec{U} \rangle \vec{v} \left[\vec{K}^{-1} [\frac{\partial \psi}{\partial \vec{k}} + \frac{\partial \vec{c}_g}{\partial x_a} \vec{v} + \frac{\partial \vec{u}_r}{\partial y_r} v_r + 0.5 u_a] \right] \left[\frac{\partial \psi}{\partial \omega} \right]$$

$$\frac{\vec{c}_g(\vec{K})\vec{v} + j.0.5\omega_0^{-1}}{[\vec{c}_g(\vec{K})\vec{v}]^2 + [0.5\omega_0^{-1}]^2} + j(6.10^{-3}.\vec{K}^{-4})(\frac{R}{V})v_r \tag{7}$$

where, $\overrightarrow{\langle U \rangle}$ is the mean current velocity, $\vec{u}_r$ is the current flow along the range direction while $\vec{u}_a$ is current gradient along the azimuth direction. K_r is the wave number along the range direction, $\vec{K}$ is the spectra wave vector, ω_0 is the angular wave frequency, $\vec{c}_g$ is the group velocity, ψ is the wave spectra energy, v stands for the Volterra kernel frequency along the azimuth and range directions and *R/V* is the range to platform velocity ratio.

Then, the domain frequency of TOPSAR data $I_{TOPSAR}(v, \Psi)$ can be expressed by using Volterra model for ABE into equation 6

$$I_{TOPSARV}(v, \Psi) = FFT[(\Psi_0(a,r) + \int Y(n)). \sum_{N=0}^{+\infty} \frac{1}{n!}(j\frac{R}{V}u_r(a,r))^N] \tag{8}$$

where *N = 1,2,3,……….k* and $I_{TOPSARV}(v, \Psi)$ represents Volterra kernels for the TOPSAR image in frequency domain in which can be used to estimate mean current flow $\vec{U}_r(0,r)$ in the range direction *(r)* with the following expression (Inglada and Garello, 2002)

$$I_{TOPSARV} = \vec{U}_r(0,r).H_{1r}(v_a, v_r) \tag{9}$$

The mean current movement along the range direction can be calculated by using the formula was proposed by Vogelzang et al. (1997)

$$\vec{U}_r(v_a, v_r) = \frac{FFT\left[\prod_{j=1}^{i} I_{TOPSARV}(t) \right]}{H_{1r}(v_a, v_r)} \tag{10}$$

where $FFT\left[\prod_{j=1}^{i} I_{TOPSARV}(t)\right]$ is the linearity of the Fourier transform for the input TOPSAR

image intensity $I_{TOPSARV}(t)$ i.e. t is time domain. The inverse filter $P(v_a, v_r)$ is used since $H_{1r}(v_a, v_r)$ has a zero for $\vec{U}_r(v_a, v_r)$ which indicates that the mean current velocity should have a constant offset. The inverse filter $P(v_a, v_r)$ can be given as

$$P(v_a, v_r) = \begin{cases} [H_{1r}(v_a, v_r)]^{-1} & if(v_a, v_r) \neq 0, \\ 0 & \text{Otherwise.} \end{cases} \qquad (11)$$

Then, the continuity equation is used to estimate the water depth as given by Vogelzang et al. (1992)

$$\frac{\partial \zeta}{\partial t} + \nabla.\{(d + \zeta)\vec{U}_r(0, v_r)\} = 0 \qquad (12)$$

where ζ is the surface elevation above the mean sea level, which is obtained from the tidal table, t is the time and d is the local water depth. The real current data was estimated from the Malaysian tidal table of 6 December, 1996 (Malaysian Department of Survey and Mapping 1996).

4.3 The fuzzy B-splines method

The fuzzy B-splines (FBS) are introduced allowing fuzzy numbers instead of intervals in the definition of the B-splines. Typically, in computer graphics, two objective quality definitions for fuzzy B-splines are used: triangle-based criteria and edge-based criteria (Marghany et al., 2009a). A fuzzy number is defined using interval analysis. There are two basic notions that we combine together: confidence interval and presumption level. A confidence interval is a real values interval which provides the sharpest enclosing range for current gradient values.

An assumption μ -level is an estimated truth value in the [0, 1] interval on our knowledge level of the gradient current (Anile 1997). The 0 value corresponds to minimum knowledge of gradient current, and 1 to the maximum gradient current. A fuzzy number is then prearranged in the confidence interval set, each one related to an assumption level $\mu \in [0, 1]$. Moreover, the following must hold for each pair of confidence intervals which define a number: $\mu \succ \mu' \Rightarrow d \succ d'$.

Let us consider a function $f : d \to d'$, of N fuzzy variables $d_1, d_2, ..., d_n$. Where d_n are the global minimum and maximum values of the water depth of the function on the current gradient along the space. Based on the spatial variation of the gradient current, and water depth, the fuzzy B-spline algorithm is used to compute the function f (Marghany et al., 2010).

Marghany et al., (2010) assumed that $d(i,j)$ is the depth value at location i,j in the region D where i is the horizontal and j is the vertical coordinates of a grid of m times n rectangular cells. Let N be the set of eight neighbouring cells. The input variables of the fuzzy are the amplitude differences of water depth d defined by (Anile et al. 1997):

$$\Delta d_N = d_i - d_0, N = 1,\ldots\ldots,8 \tag{13}$$

where the d_i, N=1, 8 values are the neighbouring cells of the actually processed cell d_0 along the horizontal coordinate i. To estimate the fuzzy number of water depth d_j which is located along the vertical coordinate j, we estimated the membership function values μ and μ' of the fuzzy variables d_i and d_j, respectively by the following equations were described by Rövid et al. (2004)

$$\mu = \max\left\{\min\left\{m_{pl}(\Delta d_i) : d_i \in N_i\right\}; N = 1\ldots,9\right\} \tag{14}$$

$$\mu' = \max\left\{\min\left\{m_{LNl}(\Delta d_i) : d_i \in N_i\right\}; N = 1\ldots,9\right\} \tag{15}$$

where m_{pl} and m_{LNl} correspond to the membership functions of fuzzy sets. From equations 11 and 12, one can estimate the fuzzy number of water depth d_j

$$d_j = d_i + (L-1)\Delta\mu \tag{16}$$

where $\Delta\mu$ is $\mu - \mu'$ and $L = \{d_1,\ldots\ldots,d_N\}$. Equations 15 and 16 represent water depth in 2-D, in order to reconstruct fuzzy values of water depth in 3-D, then fuzzy number of water depth in z coordinate is estimated by the following equation proposed by Russo (1998) and Marghany et al., (2010),

$$d_z = \Delta\mu MAX\{m_{LA}\left|d_{i-1,j} - d_{i,j}\right|, m_{LA}\left|d_{i,j-1} - d_{i,j}\right|\} \tag{17}$$

where d_z fuzzy set of water depth values in z coordinate which is function of i and j coordinates i.e. $d_z = F(d_i, d_j)$. Fuzzy number F_O for water depth in i,j and z coordinates then can be given by

$$F_O = \{\min(d_{z_0},\ldots\ldots,d_{z_\Omega}), \max(d_{z_0},\ldots\ldots,d_{z_\Omega})\} \tag{18}$$

where Ω =1, 2, 3, 4,

The fuzzy number of water depth F_O then is defined by B-spline in order to reconstruct 3-D of water depth. In doing so, B-spline functions including the knot positions, and fuzzy set of control points are constructed. The requirements for B-spline surface are set of control points, set of weights and three sets of knot vectors and are parameterized in the p and q directions.

Following Marghany et al., (2009b) and Marghany et al., (2010), as in the Volterra algorithm, data are derived from the TOPSAR polarised backscatter images by the application of a 2-dimensional fast Fourier transform (2DFFT). First, each estimated current data value in a fixed kernel window size of 512 x 512 pixels and lines is considered as a triangular fuzzy number defined by a minimum, maximum and measured value. Among all the fuzzy numbers falling within a kernel window size, a fuzzy number is defined whose range is given by the minimum and maximum values of gradient current and water depth along each kernel window size. Furthermore, the identification of a fuzzy number is acquired to summarize the estimated water depth data in a cell and it is characterized by a suitable membership function. The choice

of the most appropriate membership is based on triangular numbers which are identified by minimum, maximum, and mean values of water depth estimated by continuity equation. Furthermore, the membership support is the range of water depth data in the cell and whose vertex is the median value of water depth data (Anile et al. 1997).

5. Three-dimensional ocean bathymetry from TOPSAR data

Figure 3 shows the signature of the underwater topography. The signature of underwater topography is obvious as frontal lines parallel to the shoreline. The backscattered intensity is damped by -2 to -10 dB compared to the surrounding water environment in L –band with HH polarization and -6 to -14 dB in C-band with VV polarization data (Fig. 3).

(a)   (b)
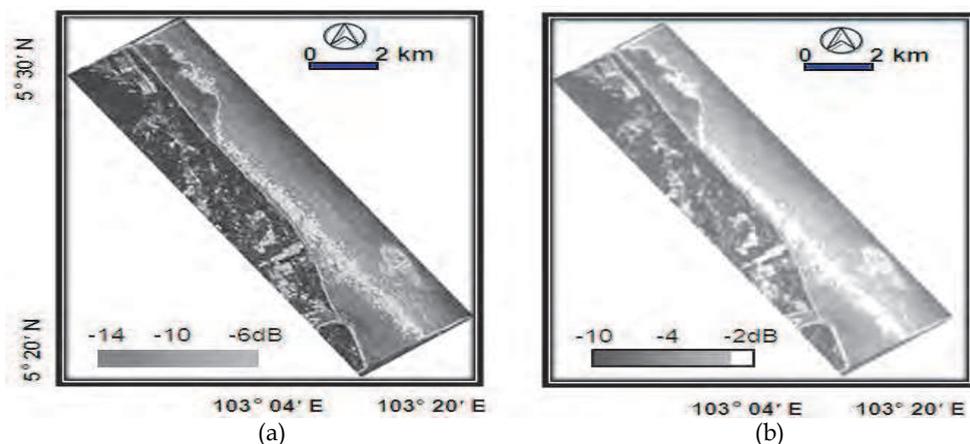
Fig. 3. Bathymetry Signature with Different Bands of (a) C_{VV} and (b) L_{HH} bands.

Figure 4 shows the clearer bathymetry signature is extracted by utilizing anisotropic diffusion algorithm. L_{HH} band has clear bathymetry feature than C_{VV} band. In fact, anisotropic diffusion algorithm is able to extract boundary edge for both horizontal and vertical direction. Otherwise said, it is synthesized boundary edge (Maeda et al. 1997 and Marghany et al., 2009b). In this regard, anisotropic diffusion resembles the process that creates a scale-space, where an image generates a parameterized family of successively more and more blurred images based on a diffusion process. Each of the resulting images in this family are given as a convolution between the image and a 2-D isotropic Gaussian filter, where the width of the filter increases with the parameter (Fig. 4). This diffusion process is a linear and space-invariant transformation of the original image. Anisotropic diffusion is a generalization of this diffusion process: it produces a family of parameterized images, but each resulting image is a combination between the original image and a filter that depends on the local content of the original image. As a consequence, anisotropic diffusion is a non-linear and space-variant transformation of the original image.

In addition, both C_{vv} and L_{HH} bands show bathymetry signature is concided with water depths which are ranged between 5 m to 20 m (Fig.4). The results show the potential of TOPSAR data for ocean bathymetry reconstruction where TOPSAR L_{HH} band backscatter across bathymetry signature pixels agrees satisfactorily with previous published results

(Vogelzang et al. 1992; Inglada and Garello 1999; Marghany et al., 2007). This is due to the fact that the ocean signature of the boundary is clear in the brightness of a radar return, since the backscatter tends to be proportional to wave height (Vogelzang et al. 1992). In C-band with VV polarization, this feature is clearly weaker than at L–band with HH polarization. In fact, L_{HH} band has higher backscatter value of 2 dB than C_{VV} band. In this context, it is possible that the character of the current gradient is such that the L_{HH} band surface Bragg waves are more strongly modulated than for C_{VV} band. This may provide an explanation for weaker bathymetric signatures at C_{VV} band. The finding is similar to that of Romeiser and Alpers (1997).
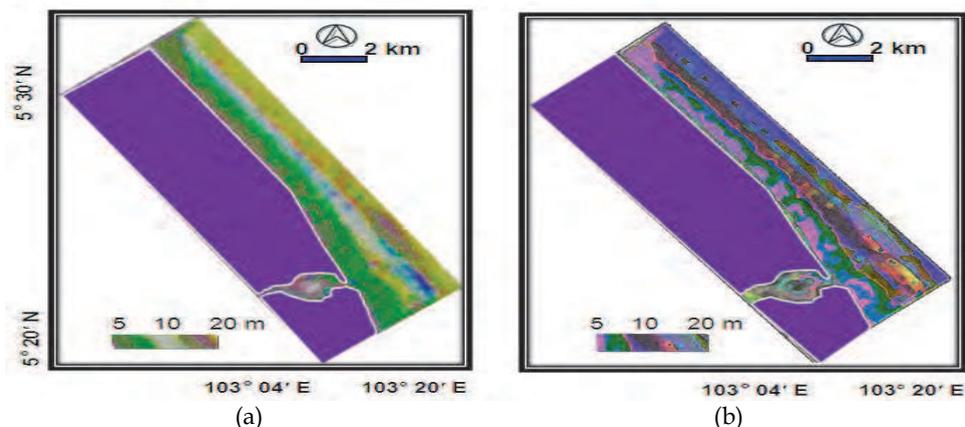
Fig. 4. Result of anisotropic diffusion algorithm for bathymetry signature from (a) C_{VV} and (b) L_{HH} bands.

Comparison between Figs. 5 and 6 showed that the L_{HH} band captured a stronger tidal current flow than the C_{VV} band. The maximum tidal current velocity simulated from the L_{HH} band is 1.6 m s^{-1} while the ones is simulated from C_{VV} band is 1.4 m s^{-1}. This is because different bands with differrent polarizations. The major axis of tidal current is towards the south and approximately moving parallel to shoreline (Figs. 5 and 6). In addition, it is obvious that both bands are imaging the major axis of tidal current in the range direction.

This is because December represents the northeast monsoon period as the coastal water currents in the South China Sea tend to move from the north towards the south (Marghany 1994). The travelling the of current is caused by the weak non-linearity due to the smaller value of R/V. The weak non-linearity was assisted by the contribution of the linear Volterra kernels of the range current. This means that the range current will be equal to zero when the Volterra kernels $H_{1y}(v_x, v_y)$ of the frequency domain has a zero for $|v_x$ and $v_y|$. However, the inversion of the linear kernel of the Volterra algorithm allowed us to map the current movements along the range direction. This result confirms the study of Inglada and Garello (1999). The results of the Volterra algorithm showed that there was an interaction between water flow from the mouth of the Kuala Terengganu River and the near South China Sea water flow which appeared to be close to the mouth of the Kuala Terengganu River (Marghany 2009 and Marghany et al., 2010).
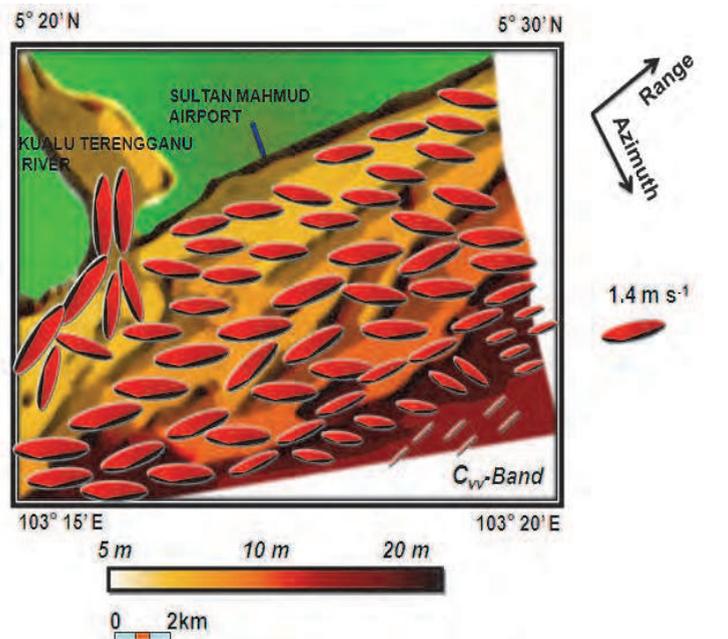
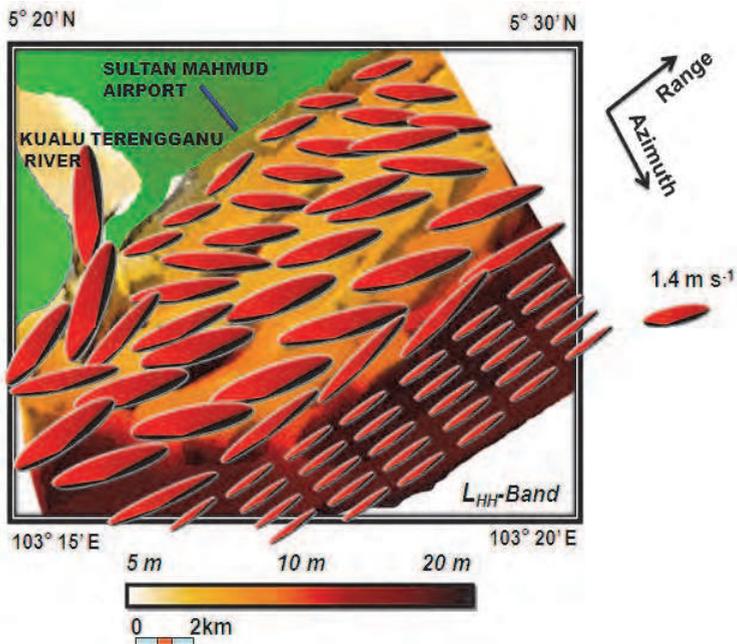Fig. 5. Tidal Current Ellipses Simulated from C_{VV} band.

Fig. 6. Tidal Current Ellipses Simulated from L_{HH} band.

In addition, during the data acquisition time, the wind was blowing at about 8 m s^{-1} from northeast and swell system was propagated from the northeast. In this regard, the quality of bathymetry map simulated from C-band degrades because the image modulation become weaker relative to the speckle noise, and they are smeared out over a larger area due to the effect of long waves, which also add noise. As L-band data suffer less from these drawbacks, using of L-band provides more accurate results. In fact L-band has higher signal-to-noise ratio compared to C band. This confirms the study of Vogelzang (1997). Furthermore, the HH polarization has a larger tilt modulation compared to the VV polarization. Tilt modulation explains that the Bragg scattering is dependent on the local incident angle. The long wavelength of L-band HH polarization modulates this angle, hence modifying the Bragg resonance wave length. It might be due to the fact that the first – order Bragg Scattering gives good results for long radar wavelengths (L-band), but for shorter radar wavelength (C-band) the effects of waves longer than the Bragg waves must be taken into account (Shuchman et al., 1985 and Romeiser and Alpers, 1997). This could be due to strong current flow from the mouth river of the Kuala Terengganu. This study confirms the studies of Li et al., (2009) and Marghany et al., (2010).

Figure 7 shows the comparison between the 3-D bathymetry reconstruction from the topographic map , the L_{HH} band data, and the C_{VV} band data. 3-D topographic map was created using fuzzy concept by converting the 2-D topographic map into fuzzy interval number of [0,1]. It is obvious that the coastal water bathymetry along the Sultan Mahmud Airport has a gentle slope and the bathymetric contours are parallel to the shoreline. Close to the river mouth, the bathymetry at this location shows a sharp slope. The L_{HH} band captured a more real bathymetry pattern than the C_{VV} band. Further, Fig. 8 shows a clear discrimination between smooth and rough bathymetry where the symmetric three-dimensional structure of the bathymetry of a segment of a connecting depth. This can be noticed in areas A, B, C, D, E in real and L_{HH} band data compared to C_{VV} band. Smooth sub-surfaces appear in Figure 6 where the near-shore bathymetric contour of 5 m (area E) water depth runs nearly parallel in 3D-space to the coastline which is clear in Figure 6. Further, statistical analysis using regression model (Fig. 7) has confirmed that L_{HH} band tends to get closer to the true mean of real bathymetry map i.e. it is actual measured as more real, as compared to C_{VV} band data. A rough sub-surface structure appears in steep regions of 20 m water depth (areas of B, C, and D). This is due to the fact that the fuzzy B-splines considered as deterministic algorithms which are described here optimize a triangulation only locally between two different points (Anile et al. 1995). This corresponds to the feature of deterministic strategies of finding only sub-optimal solutions.

This result could be confirmed using linear regression model (Fig. 8). In this regard, Fig. 8a shows the regression relation between the observed bathymetry and the results obtained using the C_{VV} band TOPSAR data. Figure 8b shows a similar regression relationship for L_{HH} TOPSAR data. The scatter points in Fig. 8b are more close to the regression line than those in Fig. 8a. The bathymetry simulation from L_{HH} band with r^2 value of 0.95 and accuracy (root mean square) of ±0.023 m is more accurate than that obtained by using C_{VV} band with accuracy of (root mean square) ±0.03 m

(a)   (b)
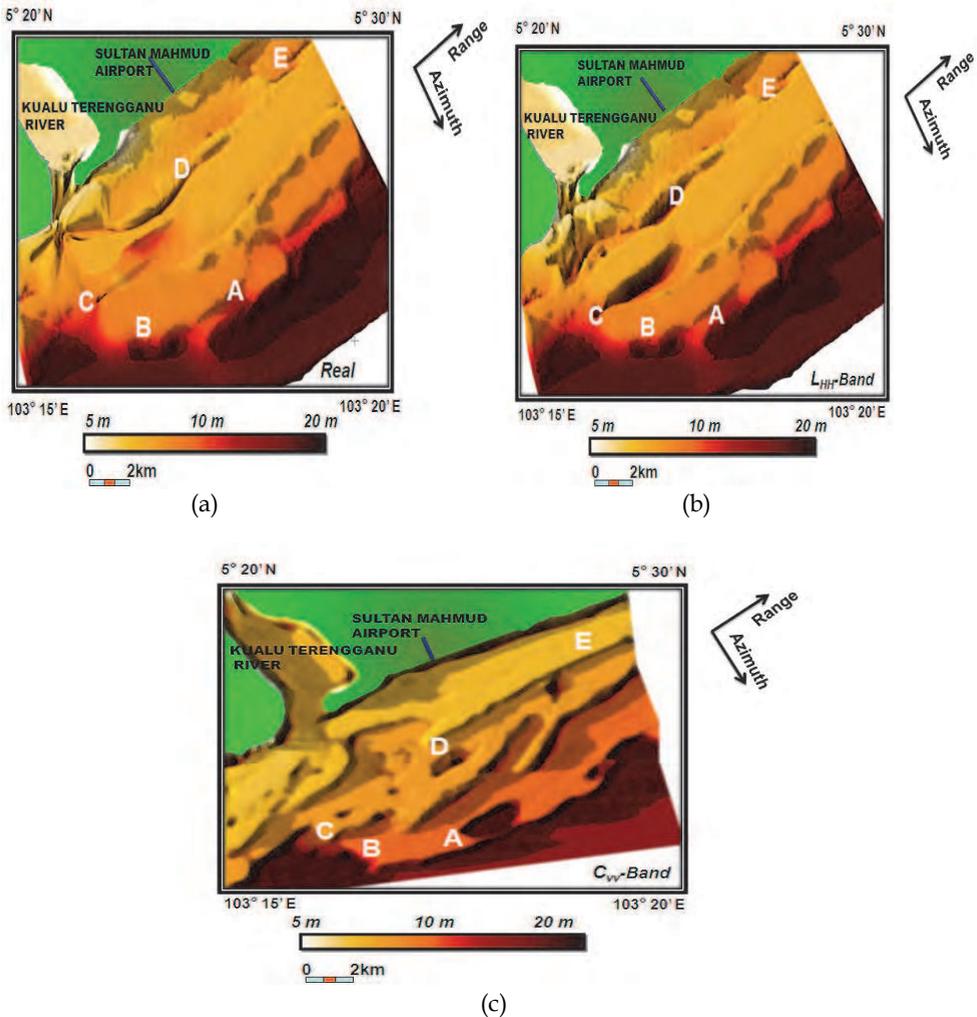

(c)

Fig. 7. Three-Dimensional Bathymetry Reconstructions from (a) Real Topography Map (b) L_{HH} Band and (c) C_{VV} Band.

It is clear that involving of fuzzy B-spline in 3-D bathymetric mapping has produced accurate bathymetry visualization. Therefore, the sharp visualization of 3-D bathymetry with the different TOPSAR polarised bands and real data due to the fact that each operation on a fuzzy number becomes a sequence of corresponding operations on the respective μ-levels, and the multiple occurrences of the same fuzzy parameters evaluated as a result of the function on fuzzy variables (Anile, 1997, Anile et al. 1997). It is very easy to distinguish between smooth and jagged bathymetry. Typically, in computer graphics, two objective quality definitions for fuzzy B-splines were used: triangle-based criteria and edge-based criteria. Triangle-based criteria follow the rule of maximization or minimization,

respectively, of the angles of each triangle (Fuchs et al. 1997) which prefers short triangles with obtuse angles. This finding confirms the studies of Keppel (1975), Anile (1997), and Marghany et al., (2010).
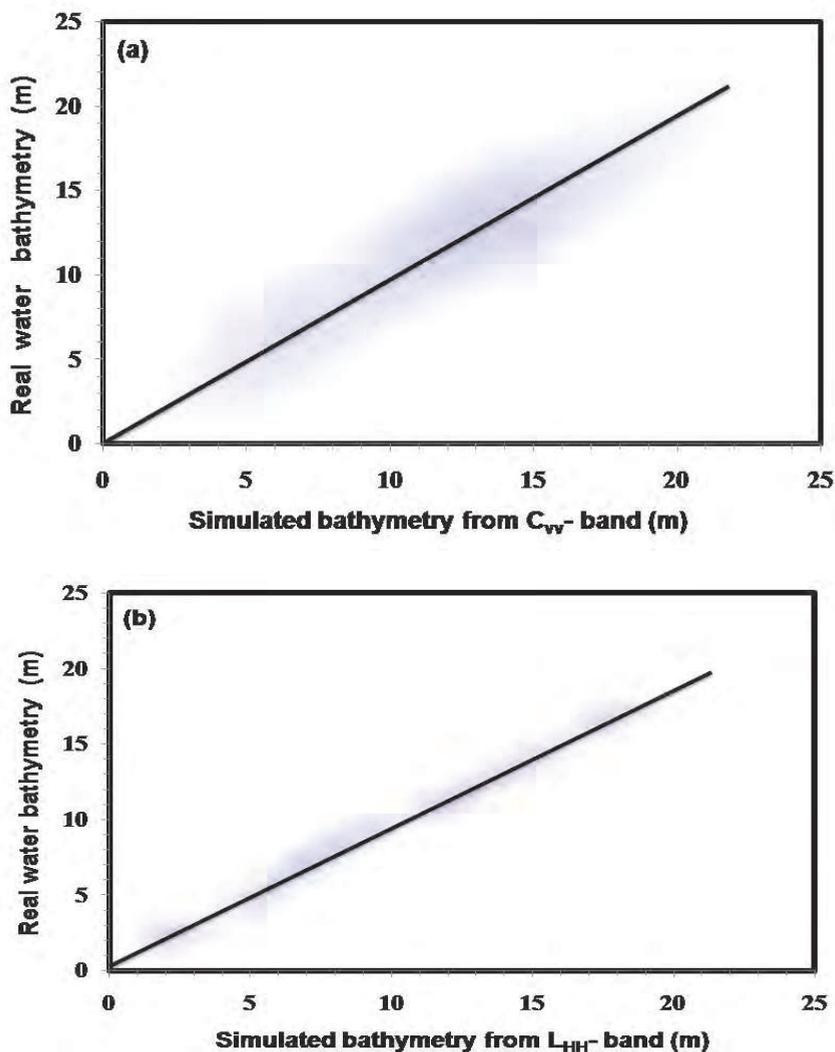

Fig. 8. Regression model between real water bathymetry from bathymetry Chart and (a) water Bathymetry from C_{VV} band ($r^2=0.85$; $y=0.95x+1.89$;$rms=\pm0.03$ m) and (b) L_{HH} band ($r^2=0.95$; $y=1.01 x+0.121$; rms=±0.023 m).

The three-dimensional bathymetry construction is not similar to the study of Inglada and Garello (1999), such that in the latter the bathymetry was constructed in the shallow sand waves (Garello 1999)due to the limitation of the inversion of the linear kernel of the Volterra

algorithm. The integration of the inversion of the Volterra algorithm with fuzzy B-splines improved the three-dimensional bathymetry reconstruction pattern. The result obtained in this study disagrees with the previous study by Inglada and Garello (1999 and 2002) who implemented two-dimensional Volterra model to SAR data. 3-D object reconstruction is required to model variation of random points which are function of x, y, and z coordinates rather than using two coordinates i.e. (x, y). In addition, finite element model is required to discretize two-dimensional Volterra and continuity models in study of Inglada and Garello (1999 and 2002) to acquire depth variation in SAR image without uncertainty. Previous studies done by Alpers and Hennings (1984); Shuchman et al. (1985); Vogelzang (1997); Romeiser and Alpers (1997); Hesselmans et al., (2000); and Li et al., (2009) were able to model spatial variation of sand waves.

Splinter and Holman (2009) have developed algorithm that is based on the changing direction of refracting waves to determine underlying bathymetry gradients function of the irrotationality of wavenumber condition. In this context, Splinter and Holman (2009) claimed that depth dependences are explicitly introduced through the linear dispersion relationship. Further, they used spatial gradients of wave phase and integrated times methods between sample locations (a tomographic approach) to extract wave number and angle from images. They found that synthetic bathymetries of increasing complexity showed a mean bathymetry bias of 0.01 m and mean rms of 0.17 m. Nevertheless, refraction-based algorithm has limitations in which it can be applied only within 500 m from the shoreline. In this circumstance, bathymetry of complex rough sea surface interaction cannot be determined. This suggests that the refraction-based algorithm is best suited for shorter period swell conditions in intermediate water depths such as a semi-enclosed sea. Further, the refraction-based algorithm cannot be implemented in SAR data. In fact, the shortest wavelength less than 50 m cannot be estimated in SAR data due to the limitation of using two dimensional (2D) Fourier transform (Romeiser and Alpers, 1997).

In this study, fuzzy B-spline algorithm produced 3-D bathymetry reconstruction without existence of shallow sand waves. In fact fuzzy B-spline algorithm is able to keep track of uncertainty and provide tool for representing spatially clustered depth points. This advantage of fuzzy B-spline is not provided in Volterra algorithm and 1-D or 2-D continuity model.

6. Conclusions

Coastal bathymetry is tremendous information for coastal engineering, coastal navigation, economic activities, security and marine environmental protection. Single- or multi-beam ship-borne echo sounders are the conventional techniques used to map ocean bathymetry. Indeed, SAR data can reduce the root mean square error of bathymetry mapping from conventional methods by overall of 40 %. In this paper, we address the question despeckles' impact on the accuracy of depth determination in TOPSAR data without needing to include any sounding data values. This verified with airborne SAR data (namely the TOPSAR) using integration of the anisotropic diffusion algorithm ,the Volterra kernel and the fuzzy B-spline algorithm. Incidentally, the inverse of Volterra algorithm then performed to retrieve 2-D tidal current flows from C_{VV} and L_{HH} bands. Besides, the 2-D continuity equation then used to retrieve the water depth. To retrieve 3-

D bathymetry pattern, the fuzzy B-spline has performed to 2-D water depth information which estimated using 2-D continuity equation.

The study shows that anisotropic diffusion algorithm provides a clear bathymetry signature in L_{HH} band data compared to C_{VV} band data. Further, the maximum tidal current flow simulated from the C_{VV} band was 1.4 m s^{-1} while the ones was simulated from L_{HH} band was 1.6 m s^{-1}. This was assisted L_{HH} band to capture more accurately bathymetry features with r^2 value of 0.95, standard error mean of ±0.023 m. In comparison with SAR satellite data, L_{HH} band performs better because of TOPSAR data acquired with HH-,VV-, HV- and VH-polarized signals from 5 m x 5 m pixels. Further, TOPSAR data provides digital elevation model (DEM) with RMSE ± 1 m in the near range to greater than ±3 m in the far range. Conventional survey, however, has lower resolution than L_{HH} band. Indeed, the conventional survey cover swath width of 37.5 m to 400 m. Nevertheless, L_{HH} band has limitation to detect more than 20 m water depth.

It can be said that the L_{HH} band provides a better approximation to the real shallow bathymetry than does the C_{VV} band. In conclusions, the integration between anisotropic diffusion algorithm, the Volterra algorithm and the fuzzy B-splines could be an excellent tool for 3-D bathymetry determination from TOPSAR polarized data.

7. References

Alpers, W., and Hennings, I., (1984). A theory of the imaging mechanism of underwater bottom topography by real and synthetic aperture radar, *Journal of Geophysical Research*, 89, 10,529-10,546.

Anile, A. M, (1997). *Report on the activity of the fuzzy soft computing group*, Technical Report of the Dept. of Mathematics, University of Catania, March 1997, 10 pages.

Anile, AM, Deodato, S, Privitera, G, (1995) *Implementing fuzzy arithmetic*, Fuzzy Sets and Systems, 72,123-156.

Anile, A.M., Gallo, G., Perfilieva, I., (1997). *Determination of Membership Function for Cluster of Geographical data.* Genova, Italy: Institute for Applied Mathematics, National Research Council, University of Catania, Italy, October 1997, 25p., Technical Report No.26/97.

Forster, B.C., (1985). Mapping Potential of Future Spaceborne Remote Sensing System. Procs. of 27th Australia Survey Congress, Alice Springs, Institution of Surveyors, Australia, Australia, 109-117.

Fuchs, H. Z.M. Kedem, and Uselton, S.P., (1977). Optimal Surface Reconstruction from Planar Contours. *Communications of the ACM*, 20, 693-702.

Guenther, G.C., Cunningham, A.G., LaRocque, P. E., and Reid, D. J. (2000). Proceedings of EARSeL-SIG-Workshop LIDAR,Dresden/FRG,EARSeL , Strasbourg, France,June 16 – 17, 2000.

Hesselmans, G.H, G.J Wensink C.G. V. Koppen, C. Vernemmen and C.V Cauwenberghe (2000). Bathymetry assessment Demonstration off the Belgian Coast-Babel. The Hydrographical Journal . 96: pp.3-8.

Inglada, J. and Garello R.,(1999). Depth estimation and 3D topography reconstruction from SAR images showing underwater bottom topography signatures. In *Proceedings of*

Geoscience and Remote Sensing Symposium, 1999, *IGARSS'99, Hamburg, Germany, 28 June-2 July 1999, IEEE Geoscience and Remote Sensing Society, USA* . 2:pp. 956-958.

Inglada, J. and Garello, R., (2002). On rewriting the imaging mechanism of underwater bottom topography by synthetic aperture radar as a Volterra series expansion. IEEE Journal of Oceanic Engineering. 27, pp: 665-674.

Keppel, E. (1975). Approximation Complex Surfaces by Triangulations of Contour Lines. *IBM Journal of Research Development*, 19, pp: 2-11.

Lee, J. S., D. Schuler, T. L. Ainsworth, E. Krogager, D. Kasilingam, M.A. and Boerner, W.M., (2002). On the estimation of radar polarization orientation shifts induced by terrain slopes, IEEE Transactions on Geosciences and Remote Sensing, 40, pp: 30–41.

Li, X., L., Qing Xu, and Pichel, W. G., (2009). Sea surface manifestation of along-tidal-channel underwater ridges imaged by SAR. IEEE Transactions on Geosciences and Remote Sensing. 8, pp: 2467-2477.

Lyzenga, D.R., P. M. Norman, and Fred, J. T., (2006). Multispectral bathymetry using a simple physically based Algorithm. IEEE Transactions on Geosciences and Remote Sensing, 8, pp: 2251-2259.

(Malaysian Department of Survey and Mapping 1996). "Chendering". In tidal table. Pp. 241-264.

Marghany, M., (1994). Coastal Water Circulation off Kuala Terengganu, Malaysia". MSc. Thesis Universiti Pertanian Malaysia (now Universiti Putra Malaysia).

Marghany, M., (2005).Fuzzy B-spline and Volterra algorithms for modelling surface current and ocean bathymetry from polarised TOPSAR data. *Asian Journal of Information Technology.* 4, pp: 1-6.

Marghany M., and Hashim, M.,(2006). Three-dimensional reconstruction of bathymetry using C-band TOPSAR data. Photogrammetrie Fernerkundung Geoinformation. pp: 469-480.

Marghay, M., M., Hashim and Crackenal, A., (2007). 3D Bathymetry Reconstruction from AIRBORNE TOPSAR Polarized Data. In: Gervasi, O and Gavrilova, M (Eds.): Lecture Notes in Computer Science. Computational Science and Its Applications – ICCSA 2007, ICCSA 2007, LNCS 4705, Part I, Volume 4707/2007, Springer-Verlag Berlin Heidelberg, pp. 410–420, 2007.

Marghany M (2009). Volterra - Lax-wendroff algorithm for modelling sea surface flow pattern from Jason-1 satellite altimeter data. Lecture Notes in Computer Science (including subseries Lecture Notes in Artificial Intelligence and Lecture Notes in Bioinformatics) Volume 5730 LNCS, 2009, Pages 1-18.

Marghany, M. S., Mansor and Hashim, M., (2009a). Geologic mapping of United Arab Emirates using multispectral remotely sensed data. American J. of Engineering and Applied Sciences. 2, pp: 476-480.

Marghany,M., M. Hashim and Cracknell A (2009b). 3D Reconstruction of Coastal Bathymetry from AIRSAR/POLSAR data. Chinese Journal of Oceanology and Limnology.Vol. 27(1), pp.117-123.

Marghany, M. and M. Hashim (2010). Lineament mapping using multispectral remote sensing satellite data. International Journal of the Physical Sciences Vol. 5(10), pp. 1501-1507.

Marghany, M., M. Hashim and Cracknell A. (2010). 3-D visualizations of coastal bathymetry by utilization of airborne TOPSAR polarized data. *International Journal of Digital Earth*, 3(2):187 – 206.

McBean, E.A., and Rovers, F.A., (1998), Statistical procedures for analysis of environmental monitoring data and risk assessment. Prentice Hall PTR Environment and Engineering Series, Vol. 3. Upper Saddle River, New Jersey 07450. pp. 33-35.

Maeda, J., Iizawa, T., Tohru,I., and Suzuki,Y., (1997). Accurate segmentation of noisy Images Using Anisotropic Diffusion and linking of Boundary edge. IEEE TENCON-Speech and Image Technology for Computing and Telecommunications, Vol. 1,279-282.

Melba M., Kumar S., Richard M.R., Gibeaut J.C. and Amy N., (1999), Fusion of Airborne polarmetric and interferometric SAR for classification of coastal environments. *IEEE Transactions on Geosciences and Remote Sensing*, 37, pp: 1306-1315.

Mills, G. B., (2006) NOAA, Office of Coast Survey, Hydrographic Surveys Division, 1315 East-West Highway, Station 6859, Silver Spring, Maryland, USA 20910-3282. (Url: http://chartmaker.ncd.noaa.gov/hsd/ihr-s44.pdf, accessed December 2006).

Perona, P. and Jitendra Malik (1987). "Scale-space and edge detection using anisotropic diffusion". Proceedings of IEEE Computer Society Workshop on Computer Vision,. pp. 16–22.

Perona,P. and Jitendra Malik (1990). "Scale-space and edge detection using anisotropic diffusion". IEEE Transactions on Pattern Analysis and Machine Intelligence, 12 (7): 629–639.

Romeiser, R. and Alpers, W., (1997), An improved composite surface model for the radar backscattering cross section of the ocean surface, 2, Model response to surface roughness variations and the radar imaging of underwater bottom topography, *Journal of Geophysical Research*, 102, pp: 25,251-25,267.

Russo, F., (1998).Recent advances in fuzzy techniques for image enhancement. IEEE Transactions on Instrumentation and measurement. 47, pp: 1428-1434.

Rövid, A., Várkonyi, A.R. andVárlaki, P., (2004). 3D Model estimation from multiple images," IEEE International Conference on Fuzzy Systems, FUZZ-IEEE'2004, July 25-29, 2004, Budapest, Hungary, pp. 1661-1666.

Sapiro,G. (2001). Geometric partial differential equations and image analysis. Cambridge University Press. p. 223.

Shuchman, R.A., Lyzenga, D.R. and Meadows, G.A. (1985). Synthetic aperture radar imaging of ocean-bottom topography via tidal-current interactions: theory and observations, *International Journal of Remote Sensing*, 6, 1179-1200.

Splinter, K.D., and Holman R.A., (2009). Bathymetry Estimation from Single-Frame images of nearshore waves. IEEE Transactions on Geosciences and Remote Sensing, 47, pp: 3151–3160.

Yu, Y., and T. A., Scott (2002), Speckle reducing anisotropic diffusion. *IEEE Transactions on Geosciences and Remote Sensing,* 11, 1260-1270.

Vogelzang, J. (1997)., Mapping submarine sand waves with multiband imaging radar, 1, Model development and sensitivity analysis, *Journal of Geophysical Research*, 102, 1163-118.1.

Vogelzang, J., Wensink, G.J., Calkoen, C.J. and van der Kooij, M.W.A. (1997). Mapping submarine sand waves with multiband imaging radar, 2, Experimental results and model comparison, *Journal of Geophysical Research*, 102, 1183-1192.

Vogelzang, J., Wensink, G.J., de Loor, G.P., Peters, H.C. and Pouwels, H., (1992). Sea bottom topography with X band SLAR: the relation between radar imagery and bathymetry, *International Journal of Remote Sensing*, 13, pp: 1943-1958.

Wensink, H. and Campbell, G., (1997). Bathymetric map production using the ERS SAR. *Backscatter*, 8, pp: 17-22.
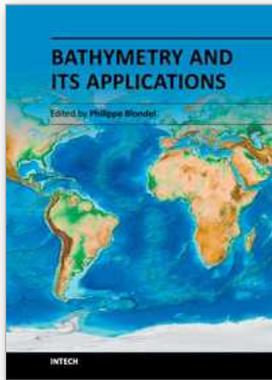
Bathymetry and Its Applications

Edited by Dr. Philippe Blondel

Bathymetry is the only way to explore, measure and manage the large portion of the Earth covered with water. This book ,presents some of the latest developments in bathymetry, using acoustic, electromagnetic and radar sensors, and in its applications, from gas seeps, pockmarks and cold-water coral reefs on the seabed to large water reservoirs and palynology. The book consists of contributions from internationally-known scientists from India, Australia, Malaysia, Norway, Mexico, USA, Germany, and Brazil, and shows applications around the world and in a wide variety of settings.

How to reference

In order to correctly reference this scholarly work, feel free to copy and paste the following:

Maged Marghany (2012). 3-D Coastal Bathymetry Simulation from Airborne TOPSAR Polarized Data, Bathymetry and Its Applications, Dr. Philippe Blondel (Ed.), ISBN: 978-953-307-959-2, InTech, Available from: http://www.intechopen.com/books/bathymetry-and-its-applications/3d-coastal-bathymetry-simulation-from-airborne-topsar-polarized-data

INTECH
open science | open minds